



Pergamon

Acta mater. 49 (2001) 2773–2781



www.elsevier.com/locate/actamat

## TRANSITION FROM NUCLEATION CONTROLLED TO GROWTH CONTROLLED CRYSTALLIZATION IN Pd<sub>43</sub>Ni<sub>10</sub>Cu<sub>27</sub>P<sub>20</sub> MELTS

J. SCHROERS<sup>1</sup>†, Y. WU<sup>2</sup>, R. BUSCH<sup>3</sup> and W. L. JOHNSON<sup>1</sup>

<sup>1</sup>California Institute of Technology, Keck Laboratory of Engineering Materials 138-78, Pasadena, CA 91125, USA, <sup>2</sup>Department of Physics and Astronomy and Curriculum in Applied and Materials Sciences, University of North Carolina, Chapel Hill, NC 27599-3255, USA and <sup>3</sup>Department of Mechanical Engineering, Oregon State University, Corvallis, OR 97331, USA

( Received 28 February 2001; received in revised form 5 April 2001; accepted 10 April 2001 )

**Abstract**—Crystallization of undercooled Pd<sub>43</sub>Ni<sub>10</sub>Cu<sub>27</sub>P<sub>20</sub> melts is studied in a differential scanning calorimeter. Isothermal experiments allow us for the first time to determine the entire crystallization kinetics of a metallic liquid as a function of time from the liquidus temperature to the glass transition temperature. The results are summarized in a time–temperature–transformation (TTT) diagram that reveals two time scales. One is given by the time to reach 1% of crystallized volume fraction and reflects the typical “nose” shape of the TTT-diagram. The other is the width of the crystallization event itself, which increases with decreasing temperature from 90 s at 793 K to 10,200 s at 623 K. Additional information about the crystallization process is gained by dividing the sample into about 300 particles that are processed simultaneously and crystallization of each individual particle can be detected. At high temperatures the onset of crystallization of individual particles are spread out over  $1.5 \times 10^5$  s, whereas all particles crystallize simultaneously below the nose and the crystallization is not distinguishable from that of one large sample. The results suggest that the dominant crystallization mechanism changes in a very narrow temperature range from a nucleation-controlled process at high temperatures to a growth-controlled process at low temperatures. © 2001 Acta Materialia Inc. Published by Elsevier Science Ltd. All rights reserved.

**Keywords:** Supercooled liquids; Crystallization; Nucleation; Bulk metallic glasses; Decomposition

### 1. INTRODUCTION

In 1984 Pd<sub>40</sub>Ni<sub>40</sub>P<sub>20</sub> has been discovered as the first bulk metallic glass (BMG) forming alloy with a critical cooling rate as low as about 1 K/s when processed in B<sub>2</sub>O<sub>3</sub> [1]. The discovery of the La- [2] and Zr- [3, 4] based alloys has triggered tremendous research activity in this area. This led to the revisit of the Pd-based alloys. By partially replacing Ni by Cu in Pd<sub>40</sub>Ni<sub>40</sub>P<sub>20</sub>, Inoue and co-workers discovered Pd<sub>40</sub>Ni<sub>10</sub>Cu<sub>30</sub>P<sub>20</sub> that shows a substantial improvement of the glass forming ability [5]. Lu *et al.* enhanced the glass forming ability even further by adjusting the Pd-composition with respect to Cu [6]. This resulted in the Pd<sub>43</sub>Ni<sub>10</sub>Cu<sub>27</sub>P<sub>20</sub> alloy, which has the lowest critical cooling rate of all BMGs thus far. The high stability of these quaternary PdNiCuP alloys against crystallization leads to a large experimentally accessible time and temperature window for investi-

gations of the transformation behavior under isothermal conditions from the supercooled (undercooled) liquid into crystalline phases. A characterization of the time scale for crystallization under isothermal conditions is given by the time–temperature–transformation (TTT) diagram. In general, a TTT-diagram describes the transformation kinetics from liquid to solid in an isothermal experiment as a function of temperature. For metallic systems TTT-diagrams have been measured so far that only depict the time to reach crystallization. The first TTT-diagram for a metallic system was measured on the bulk glass forming liquid Zr<sub>41</sub>Ti<sub>14</sub>Cu<sub>12</sub>Ni<sub>10</sub>Be<sub>23</sub> with an electrostatic levitator [7]. Very recently, PdNiCuP alloys were studied with an rf-heating apparatus and the TTT-diagrams were determined by inductively heating the samples in graphite crucibles [8, 9]. These investigations determined the time scale to reach the onset of crystallization and confirm the theoretically predicted nose shape [10]. However, the time dependence of the entire crystallization process, which is given by the time to reach the onset of crystallization and the time for the actual crystallization process to complete has not been studied over the temperature

† To whom all correspondence should be addressed. Fax: +1-626-795-6132.

E-mail address: schroers@hyperfine.caltech.edu (J. Schroers)

range from the equilibrium liquid down to the glass transition temperature,  $T_g$ . The knowledge of the progression of the crystallization with time can provide a deeper insight into the crystallization mechanism of bulk metallic glass forming liquid.

Statistical methods are powerful tools to investigate crystallization of supercooled liquids [11, 12]. One approach is to divide the sample into small particles. It was found that much deeper undercoolings can be achieved in samples consisting of a large number of small isolated droplets than in one large sample [11]. However, those studies were limited to an undercooling region that is far above the nose temperature,  $T_n$ , in the TTT-diagram. Recently, repeated undercooling experiments were performed on  $Zr_{41}Ti_{14}Cu_{12}Ni_{10}Be_{23}$  [13]. These studies suggest a different crystallization mechanism at low undercoolings above the crystallization nose, compared to high undercoolings below  $T_n$  of the TTT-diagram.

This paper reports on a differential scanning calorimetry (DSC) study of crystallization in  $Pd_{43}Ni_{10}Cu_{27}P_{20}$  melts that were processed in  $B_2O_3$ . The evolution of the crystallized volume fraction as a function of time can now be measured in the entire supercooled liquid region under isothermal conditions. A complete TTT-diagram will be determined represented by 1%, 50% and 95% crystallized volume fraction. In addition, information on the crystallization process can be gained from experiments where the sample is divided into about 300 particles that are processed at the same time.

## 2. EXPERIMENTAL PROCEDURE

Amorphous samples were prepared by inductively melting the constituents (purity ranging from 99% to 99.999%) in quartz tubes for 20 min at 1200 K followed by water quenching. During this procedure the samples were fluxed in  $B_2O_3$  that was previously dehydrated for 3 h at 1200 K. It was found earlier that fluxing the ternary PdNiP alloys with  $B_2O_3$  enhances their glass forming ability [1]. Wavelength-dispersive-spectrometer measurements were carried out to verify the composition of the samples. Glassy  $Pd_{43}Ni_{10}Cu_{27}P_{20}$  samples between 2 and 30 mg and additional  $B_2O_3$  were introduced into graphite crucibles and processed in a Perkin Elmer DSC 7 analyzer. For the statistical investigations of the crystallization process the samples were divided into about 300 particles that were between 100 and 350  $\mu m$  in diameter and processed in graphite crucibles with a mixture of  $B_2O_3$  and  $Al_2O_3$ -particles. The  $Al_2O_3$ -particles, about 50  $\mu m$  in size were used to avoid fusing of the liquid particles during processing.

## 3. RESULTS

A DSC thermogram of an isothermal crystallization event performed at 773 K, which corresponds to an undercooling of 100 K below the liquidus temperature

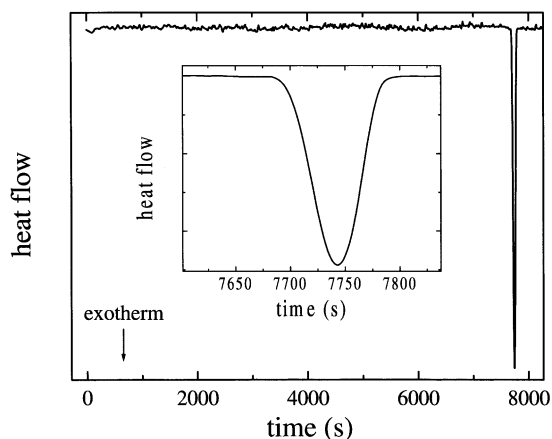


Fig. 1. DSC thermogram of an isothermal crystallization event at 773 K. A rapid crystallization event sets in after 7680 s and takes about 80 s to complete.

is shown in Fig. 1. The sample is a 3 mg particle processed in  $B_2O_3$ . For about 7680 s no detectable reaction takes place in the liquid. Thereafter, a very rapid crystallization event occurs, which is enlarged in the inset of Fig. 1. Figure 2 shows the time integrals over the isothermal DSC signals at 773 K, 723 K, 703 K, and 628 K for about 3 mg samples processed in  $B_2O_3$ . It is proportional to the crystallized volume fraction if we assume that the heat flow measured upon crystallization in the DSC is proportional to the crystallization rate. For an isothermal measurement carried out at 773 K the time to reach 1% crystallization,  $t_{1\%}$ , takes 7700 s. The time between 1% and 95% of transformation into the crystalline state is 80 s. In the following this time is referred to as the peak width of the crystallization event. By repeating this isothermal experiment, a large scatter in  $t_{1\%}$  was observed. The peak width, however, stays constant within about 50%. For 10 repetitions at 773 K,  $t_{1\%}$  varies between 96 s and  $2.3 \times 10^4$  s. In an isothermal experiment performed at 723 K crystallization occurs

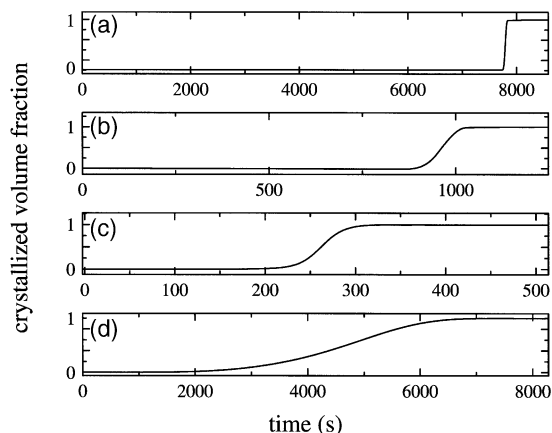


Fig. 2. Crystallized volume fraction as a function of temperature at 773 K (a), 723 K (b), 703 K (c), and 628 K (d). Note that the x-axes have different scales.

in a very similar way. The event shown in Fig. 2(b) takes place after 890 s with a peak width of 120 s. The experiment was also repeated 13 times and  $t_{1\%}$  varies between 200 and 2580 s for the fluxed samples. For both temperatures of 773 and 723 K no reaction inside the liquid can be detected before the rapid crystallization event take place.

To further investigate if the liquid remains unchanged until the occurrence of the main crystallization event, a two-step annealing experiment was performed. The samples were kept for 4000 s without crystallization at 773 K and were subsequently cooled to 723 K. The  $t_{1\%}$  for 723 K measured for this procedure does not change on average compared to the  $t_{1\%}$  measured on samples that were cooled to 723 K directly. This indicates, that the liquidus remains unchanged until the detectable crystallization event takes place at 773 K. This finding excludes processes like transient nucleation where during the time to reach crystallization an equilibrium cluster distribution would have been established. For the two step annealing the cluster distribution function would have evolved towards equilibrium during the first step. This should lead to a shorter time to reach crystallization in the subsequent second step as opposed to the experimental finding.

Crystallization at 703 K shown in Fig. 2(c) takes place more gradually compare to the crystallization event at 773 and 723 K. Even though 1% is transformed after 188 s the beginning of the exothermic reaction can already be detected after 100 s. The scatter of  $t_{1\%}$  decreases to 60 s within four experiments. At 628 K the crystallization peak broadens up to 5080 s. Very little scatter ( $\sim 400$  s) was observed within three experiments. Figure 3 depicts the scatter in the time to reach crystallization during isothermal crystallization for three temperatures, 773 K (a), 723 K

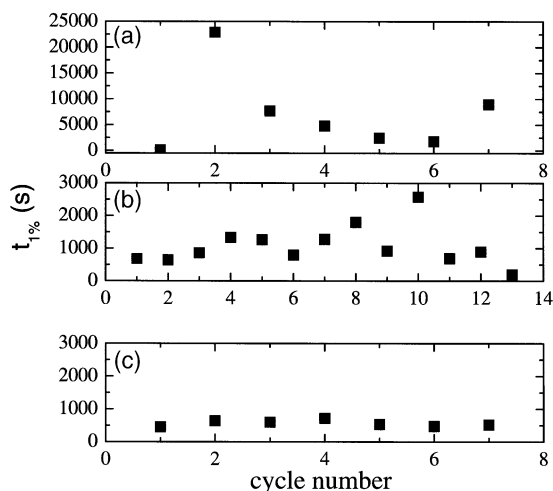


Fig. 3. Repeated undercooling experiments performed at 773 K (a), 723 K (b) and 653 K (c). A large scatter for temperatures above 720 K was observed in the time to reach crystallization from one cycle to another compare to the scatter at 653 K. Note that the y-axes have different scales.

(b) and 653 K (c). For the high temperatures above 720 K a large scatter in the time to reach crystallization was found, whereas at 653 K only very little scatter in the time to reach crystallization was observed.

The results of the isothermal crystallization experiments are summarized in the time–temperature–transformation diagram shown in Fig. 4. In this TTT diagram, the time to transform 1%, 50% and 95% volume fraction is plotted as a function of temperature. The data points represent the averages of  $t_{1\%}$ ,  $t_{50\%}$  and  $t_{95\%}$  for the performed experiments. The diagram shows the typical “nose” shape for the time to reach 1% crystallinity and this time is in good agreement to previously reported times to reach the onset of crystallization [9]. The width of the crystallization peak, however, continuously increases with decreasing temperature from 80 s at 773 K up to 10,200 s for an isothermal temperature of 623 K.

In order to investigate the observed scatter in  $t_{1\%}$ , crystallization was studied in samples that consist of many particles. Figure 5 shows the DSC thermogram of isothermal crystallization at 733 K of a sample containing about 300 particles with a diameter between 100 and 350  $\mu\text{m}$  ( $5 \times 10^{-6}$  to  $2 \times 10^{-4}$  g) that were processed in a mixture of  $\text{B}_2\text{O}_3$  and  $\text{Al}_2\text{O}_3$ . The size of the particles was chosen in such a way that the crystallization of individual particles can still be detected by DSC as shown in Fig. 5. Obviously, crystallization of the particles does not occur simultaneously but spreads out over more than  $1.5 \times 10^5$  s. After  $1.5 \times 10^5$  s the sample was cooled to room temperature and on subsequent heating a heat release that corresponds to 15% of the heat release of an entirely amorphous sample was detected. Therefore, about 15% of the particles did not crystallize even after  $1.5 \times 10^5$  s. From this measurement the number of crystallization events occurring within a time interval of 6000 s is plotted as a function of time as shown

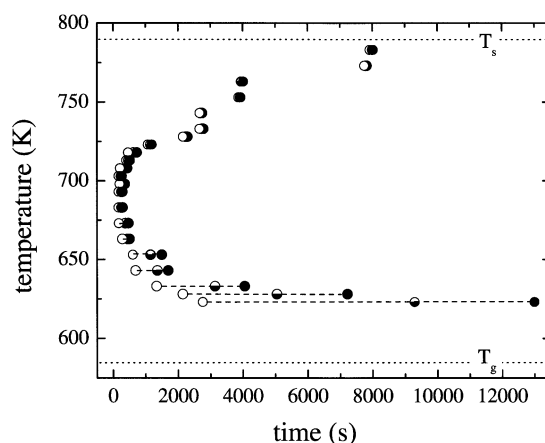


Fig. 4. Time–temperature–transformation (TTT) diagram for  $\text{Pd}_{43}\text{Ni}_{10}\text{Cu}_{27}\text{P}_{20}$ . In this diagram, the time to reach 1% ( $\circ$ ), 50% ( $\bullet$ ) and 95% ( $\bullet$ ) is shown as a function of temperature. The data points depict the average times of the performed experiments.

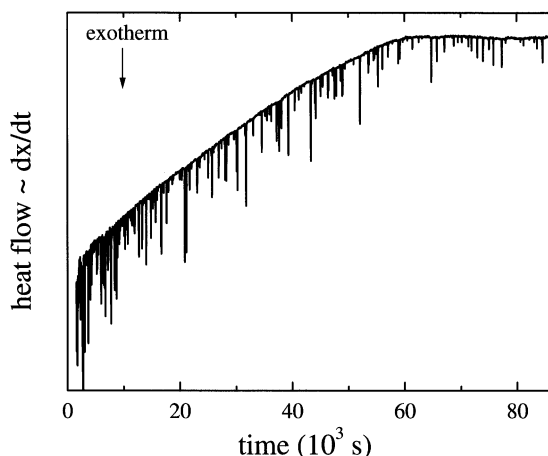


Fig. 5. DSC thermogram of 300 particles processed in  $B_2O_3$  and  $Al_2O_3$  at 733 K. The particles size is between 100  $\mu m$  and 350  $\mu m$  in diameter. Crystallization of individual particles can be detected.

in Fig. 6. The crystallization events are Poisson distributed. By plotting the number of nucleation events as a function of time the nucleation rate at 733 K can be extracted from the slope of this curve. This is shown in Fig. 7. The curve is not straight but exhibits a gradual decrease of the slope. The decline of the slope can be explained by a decreasing amount of particles that still remain liquid, and have a probability to nucleate which should follow a  $I(t) = I_{ss} \times \exp(-t/\tau)$  ( $\tau = 3 \times 10^4$ : characteristic time) time characteristic. By fitting the curve with this expression the steady state nucleation rate at 733 K can be evaluated to be  $4 \times 10^5$  nuclei/ $m^3$  s.

The particles vary in size between 100 and 350  $\mu m$ . In Fig. 8 the heat release, which is proportional to the size of the corresponding particle, is shown as a function of time at which the particle crystallized at 753 K. This plot reveals, that larger particles do on average crystallize earlier than smaller ones.

In order to study the growth mechanism the width

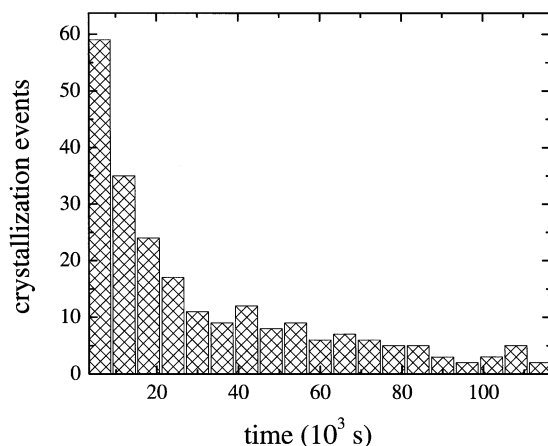


Fig. 6. Number of crystallization events in a time interval of 6000 s as a function of time, crystallized at 733 K.

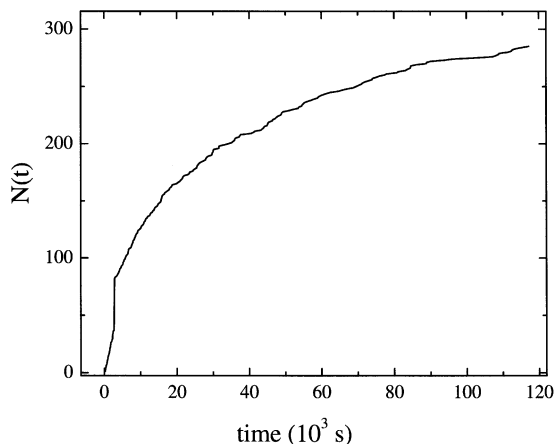


Fig. 7. Number of the crystallization events as a function of time,  $N(t)$ , crystallized at 733 K. For this sample setup a steady state nucleation mechanism results in an apparent decrease of the nucleation rate, which is the slope of this curve. This has its origin in the fact that the particles once they are crystallized no longer contribute to the potential nucleation sides, which should follow a  $I(t) = I_{ss} \times \exp(-t/\tau)$  ( $\tau = 3 \times 10^4$ : characteristic time) time characteristics. By fitting the curve with this expression,  $I_{ss}$  can be evaluated to  $4 \times 10^5$  nuclei/ $m^3$  s.

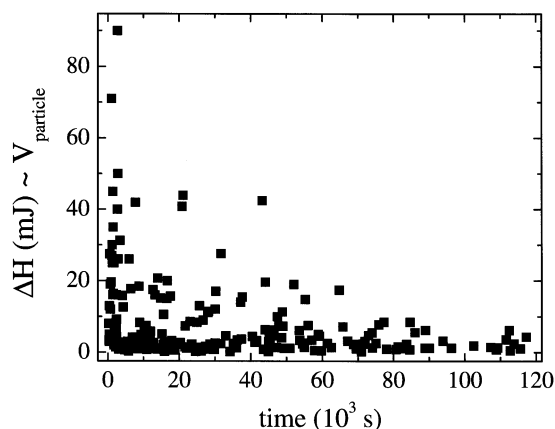


Fig. 8. Heat release of the crystallization event, which is proportional to the volume of the particles as a function of the corresponding time, at which the event occurs. On average, larger particles crystallize earlier than smaller ones.

of the crystallization event is plotted in Fig. 9 as a function of the corresponding particle volume for a temperature of 733 K. The width is given as the time between 1% and 95% crystallization. As opposed to the enormous scatter in the time to reach crystallization the peak width varies much less for the different particles but depend on the particle size. The inset depicts a  $V$  vs. peak width on a log scaled plot showing the width being proportional to  $V^{1/3}$ . This suggests that diffusion occurs over a constant length per unit time in each sample.

With the 300 particle containing sample setup isothermal crystallization studies were performed at temperatures representing the entire undercooled liquid temperature range as shown in Fig. 10. The crystalliz-

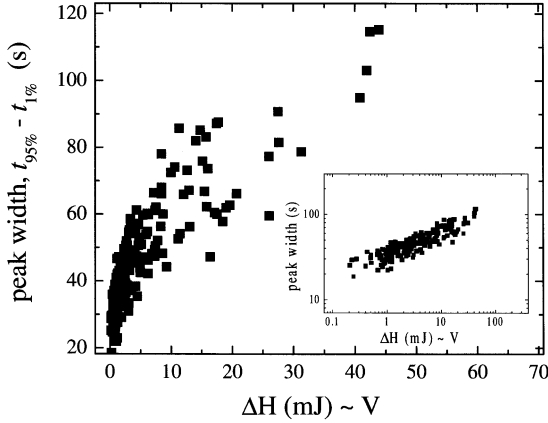


Fig. 9. Width of the crystallization peak, which we define as the time between 95% and 1% crystallization, as a function of the corresponding heat of crystallization ( $\sim$ particle volume). The inset depicts a  $V$ -peak width plot on a log scale showing the width proportional to  $V^{1/3}$ .

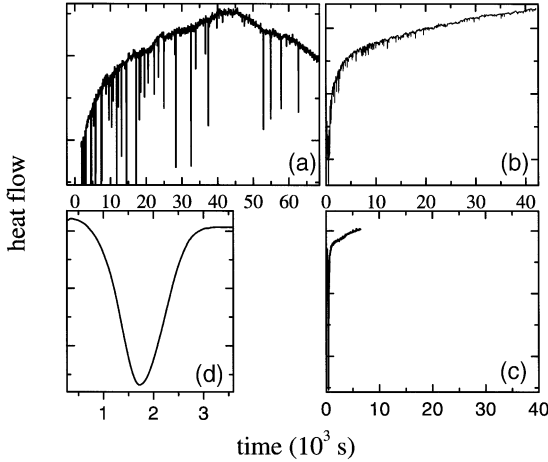


Fig. 10. Isothermal DSC thermograms measured on a sample containing about 300 particles with diameters between 100 and 350  $\mu\text{m}$ . (a) 753 K, (b) 723 K, (c) 718 K, and (d) 643 K. Between 723 K and 718 K a change in the crystallization mechanism is observed. For temperatures below 718 K crystallization occurs simultaneously in all the particles.

ation of the individual particles at 753 K is spread out over 78,000 s and 65% of the particles do not crystallize within this time period [Fig. 10(a)]. At 723 K the data look very similar. However, the time over which the events are spread out decreases to 42,000 s and only 10% did not crystallize over this time period [Fig. 10(b)]. Lowering the temperature by only 5 K to 718 K results in a very different DSC thermogram which is shown in Fig. 10(c). More than 95% of the sample crystallized simultaneously after 240 s within 200 s. The residual liquid particles do crystallize within  $3 \times 10^3$  s. Amazingly, for lower temperatures the crystallization event of the 300 particle sample can not be distinguished from a sample that contains just one bulk particle as can be seen in Fig. 10(d).

## 4. DISCUSSION

In the following we will show that conventional approaches fail to describe the time and temperature dependence of the crystallization process over the entire undercooling region. The influence of heterogeneous nucleation and phase separation on the crystallization process will be discussed especially with respect to the crossover from statistical nucleation events at high temperatures to a collective crystallization at low temperature, which occurs in a narrow temperature range.

### 4.1. Steady state nucleation

The volume fraction crystallized under isothermal conditions with a steady state nucleation rate is commonly described by the Johnson–Mehl–Avrami–Kolmogorov expression [14]

$$x(t) = 1 - \exp\left[-\frac{\pi}{3}u^3I_{\text{SS}}t^4\right] \quad (1)$$

$I_{\text{SS}}$  denotes the nucleation rate given by

$$I_{\text{SS}}(T) = \frac{A_v}{\eta(T)} \exp\left(-\frac{16\pi\sigma^3}{3k_B T \Delta g(T)^2}\right) \quad (2)$$

with  $A_v$  as a constant of the order of  $10^{32}$  Pas/( $\text{m}^3$  s),  $\eta$  the viscosity,  $\Delta g$  the difference in Gibbs free energy,  $k_B$  the Boltzmann's constant,  $\sigma$  the energy of the interface between nuclei and liquid and  $u$  the growth rate. According to Nishiyama and Inoue [15] the temperature dependence of the viscosity in  $\text{Pd}_{40}\text{Ni}_{10}\text{Cu}_{30}\text{P}_{20}$  can be described by a Vogel–Fulcher–Tamann expression,  $\eta = \eta_0 \exp(D^*T_0/(T - T_0))$ , with  $\eta_0 = 9.34 \times 10^{-3}$  Pas, the fragility parameter  $D^* = 9.25$ , and  $T_0 = 447$  K. The temperature dependence of  $\Delta g$  was estimated using Turnbull's linear expression of  $\Delta g = \Delta S_F(T_{\text{liq}} - T)$  [16], with the entropy of fusion,  $\Delta S_F = 8.03$  J/mol K and the liquidus temperature,  $T_{\text{liq}} = 873$  K [6]. The diffusion limited growth rate is described by  $u = D/(2(Dt)^{1/2})$  where  $D$  is the diffusivity. To fit the nucleation behavior, we deduced the nucleation rate at 753 K to be  $10^4$  nuclei/ $\text{m}^3$  s, since in the isothermal experiments one nucleus formed on average after about 1000 s within the sample. A nucleation rate of  $10^{16}$  nuclei/ $\text{m}^3$  s can be derived from the microstructure of a  $\text{Pd}_{40}\text{Ni}_{10}\text{Cu}_{30}\text{P}_{20}$  sample crystallized isothermally at the nose of the TTT-diagram at 673 K [8]. The temperature dependence of the diffusivity was estimated by the Stokes–Einstein equation,  $D = k_B T / (3\pi\eta a)$ , with an average atomic distance of  $a = 3.1$  Å. The fit of the initial stages of the crystallization, which can be described by  $x(t) = \pi/3 I_{\text{SS}} u t^4$  gives reasonable numbers for the interfacial energy [17] of 79 mJ and  $A_v = 1 \times 10^{30}$  Pas/ $\text{m}^3$  s.

For simplicity we assume the growth rate  $u$  to be constant and we take the constant value at  $t_{50\%}$ . This is justified by the experimental finding that the total time for crystallizing the sample is proportional to  $V^{1/3}$  (see Fig. 8) suggesting diffusion over a constant length. The crystallization rate can then be calculated by differentiating equation (1) resulting in

$$\frac{dx(t)}{dt} = \frac{4\pi}{3} u^3 I t^3 \exp\left[-\frac{\pi}{3} u^3 I_{SS} t^4\right] \quad (3)$$

for a steady state nucleation mechanism and

$$\frac{dx(t)}{dt} = \pi u^3 N t^2 \exp\left[-\frac{\pi}{3} u^3 N t^3\right] \quad (4)$$

for the case where a number  $N$  of pre-existing nuclei is present.

In Fig. 11 the calculated crystallization event according to equation (3) with the above mentioned parameters are depicted by the dotted lines. At 773 K the steady state nucleation rate amounts  $1 \times 10^2$  nuclei/m<sup>3</sup> s and the growth rate  $3 \times 10^{-9}$  m/s which give a maximum at 720,000 s with a peak width of 1,010,000 s. Those times are so far off the scale of the plot that they cannot be visualized on the plot. The same is true for the following temperatures. The calculated peak at 723 K has a maximum at 3807 s and a width of 5622 s using  $I_{SS} = 1 \times 10^{14}$  nuclei/m<sup>3</sup> s and  $u = 7 \times 10^{-10}$  m/s. For 703 K the calculated peak has a maximum at 2097 s with a peak width of 2900

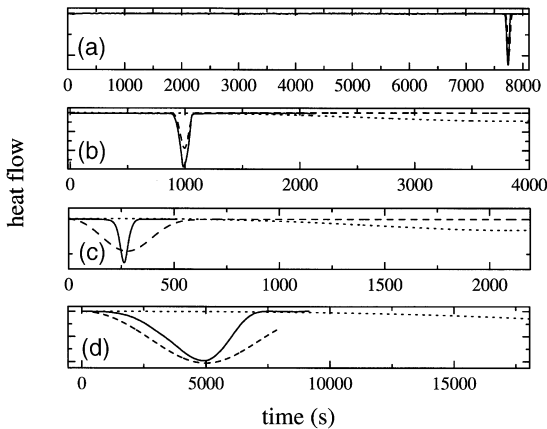


Fig. 11. DSC thermograms of isothermal crystallization events (solid line) at (a) 773 K, (b) 723 K, (c) 703 K, and (d) 628 K. The dotted line represents the calculated crystallization rate according equation (3) with  $I_{SS}$  calculated as described in the text. These data are magnified in the y-direction to compare them in the same plot to the measured events. In order to fit the crystallization peak of 773 and 723 K it was assumed that the liquid remains unchanged until about  $t_{1\%}$ . With a subsequent nucleation rate the peaks can be fitted according to equation (3) shown by the dashed lines in (a) and (b). For 628 and 703 K the dashed line represents calculations according to equation (4).

s using  $I_{SS} = 1 \times 10^{16}$  nuclei/m<sup>3</sup> s and  $u = 3.6 \times 10^{-10}$  m/s. The calculated crystallization peak at 628 K with  $I_{SS} = 1 \times 10^{17}$  nuclei/m<sup>3</sup> s and  $u = 1.6 \times 10^{-12}$  m/s has a maximum at 36,500 s with a peak width of 52,537 s. Obviously, for all temperatures these calculations do not describe the underlying crystallization mechanism.

#### 4.2. Steady state nucleation triggering further nucleation

The above considerations have clearly shown that it is not possible to describe the entire crystallization using one single steady state nucleation mechanism. However, the experimental findings lead to the conclusion that in the high temperature region the first nucleus in each of the samples forms according to a steady state nucleation process. As pointed out in Section 3, (1) the liquid remains unchanged until crystallization sets in and (2) at temperatures of 723 K and above an enormous scatter in  $t_{1\%}$  was observed, which is also reflected by the large spread of nucleation events of the samples that were fragmented into many fine particles. These crystallization events are Poisson distributed. (3) The time to reach crystallization as well as the peak width depend on the size of the particles. (4) The finding, that  $t_{1\%}$  does not change whether the sample was cooled to 723 K directly or was first kept for 4000 s at 773 K and then cooled to 723 K indicates, that the liquidus remains unchanged until the detectable crystallization event takes place at 773 K. This result excludes processes like transient nucleation where during the time to reach crystallization an equilibrium cluster distribution would have been established. For the two step annealing the cluster distribution function would have evolved towards equilibrium during the first step. This should lead to a shorter time to reach crystallization in the subsequent second step as opposed to the experimental finding.

All these four findings are indicative of steady state nucleation, which occurs also in pure metals for moderate undercooling close to the melting point. The time scale to reach the onset of crystallization ( $\sim t_{1\%}$ ) is up to three orders of magnitude larger than the time scale for each crystallization event itself, which is given by the time difference,  $t_{95\%} - t_{1\%}$ . This subsequent rapid crystallization requires either a fast growth mechanism or a sudden dramatic increase in the nucleation rate. The finding that the crystallization time is proportional to  $V^{1/3}$  indicates that diffusion occurs over a constant length per unit time like for a eutectic growth mechanism. A growth rate of  $10^{-6}$  m/s is required to result in such a rapid crystallization mechanism. The theory for eutectic growth [18] sensitively depends on unknown parameters like the partition coefficient and the slope of the liquidus curves. This makes reasonable modeling of this mechanism impossible. This view is supported by the finding that the microstructure of a sample crystallized from a high temperature shows a fairly fine

structure [19], in contrast to what is observed in pure metals or solid solutions [20]. This microstructure suggests a multiple nucleation mechanism rather than eutectic growth. If we assume that the liquid at 773 K remains unchanged until the first nucleus forms after 7200 s and a subsequent rate of  $I_{\text{sub}} = 10^{17}$  nuclei/m<sup>3</sup> s, the measured peak can be described by equation (3) as shown in Fig. 11(a) by the dashed line. The same scenario can describe the measured crystallization event at 723 K. In this case the first nucleus forms after 890 s and  $I_{\text{sub}} = 10^{18.5}$  nuclei/m<sup>3</sup> s [dashed line in Fig. 3(b)]. This apparent contradiction can be explained qualitatively in the following way. The first nucleus forms according to a low initial steady state nucleation rate, which is reflected in the time scale to reach crystallization in the TTT diagram (Fig. 4). This nucleus, then, triggers further nucleation. One explanation for this scenario is that a nucleus changes the composition in its neighborhood since the composition is close to eutectic composition where crystallization is far from polymorphic. This results in an enhancement of the nucleation rate adjacent to the nucleus, which causes a chain reaction-like process, that would lead to a much higher nucleation rate than in the initial liquid. The good agreement between the calculated and measured crystallization rate confirms that the nucleus that is initially formed by steady state nucleation triggers further nucleation and leads to fast crystallization. Even though a fixed second nucleation rate describes the form of the crystallization peak reasonably well [Fig. 11(a,b)], we cannot unambiguously decide if this (second) triggered nucleation is steady state nucleation.

### 4.3. Instability of the undercooled liquid

We observe a dramatic change of the crystallization of an ensemble of samples from individual crystallization above 723 K to collective crystallization below 718 K (Fig. 10). All 300 particles crystallize simultaneously and the signal is indistinguishable from the crystallization event of one large sample. Fluxed and unfluxed samples exhibit very similar  $t_{1\%}$ . Very little scatter is observed for  $t_{1\%}$ . An “internal clock” defines the time for crystallization below this transition region. This suggests that no considerable nucleation barrier for the formation of crystals exists below the small transition range. The spontaneously formed or pre-existing nuclei simply grow and diffusion determines the crystallization rate. Several scenarios have to be considered in order to better understand this result of the present investigation.

1. If we consider homogeneous nucleation the nucleation barrier decreases with undercooling. If the nucleation barrier becomes smaller than the thermal energy, nucleation will occur spontaneously everywhere in the undercooled liquid. “Catastrophic nucleation” is occurring and the liquid becomes unstable with respect to the forma-

tion of crystals. The crystallization of both the divided and an undivided samples is determined by the growth of these nuclei. It is however questionable that this transition can occur in a small transition interval of only 5 K. In addition, we estimate that with our thermodynamic data and a reasonable interfacial energy the nucleation barrier under the assumption of homogeneous nucleation is still two orders of magnitude higher than the thermal energy in the transition range between 718 and 723 K. Another argument against homogeneous nucleation is that catastrophic nucleation should result in a nanometer scale microstructure since nuclei consists of a small number of atoms covering the entire sample. This is in contradiction to the observed  $\mu\text{m}$  size microstructure. Therefore, homogeneous nucleation is an unlikely cause for the crystallization.

2. A factor that can also influence the stability of the undercooled melt is phase separation in the supercooled liquid. In this scenario the supercooled liquid would become unstable with respect to composition fluctuations in the vicinity of the transition region. This would happen in all samples, the large samples as well as the divided samples. The reason is, that the wavelength of a phase separation into two supercooled liquids (typically in the order of  $10^{-8}$  m) will be much smaller than even the smallest sample ( $\sim 10^{-4}$  m). If one of the supercooled liquids has a drastically reduced nucleation barrier, this destabilizes the melt with respect to the formation of crystals. It hence results in spontaneous nucleation in all samples. This could account for the merging of all crystallization peaks in the divided samples. For  $\text{Zr}_{41}\text{Ti}_{14}\text{Cu}_{12}\text{Ni}_{10}\text{Be}_{23}$  (Vit 1) it was found earlier that upon cooling from the stable melt a decomposition process occurs [21] that leads to spontaneous crystallization in distinctive regions of the supercooled liquid [22]. In the  $\text{Pd}_{43}\text{Ni}_{10}\text{Cu}_{27}\text{P}_{20}$  alloy two glass transition temperatures have been observed after annealing the material above the glass transition, indicating that decomposition processes in fact occur in the melt [23]. However, so far we have not prove that decomposition occurs in the transition region between 718 and 723 K.
3. The most likely cause for the observed crossover to collective crystallization is the influence of heterogeneous sites on the crystallization process. If we assume that heterogeneities are present in the melt, their number density and size depends on the purity of the constituents and the processing conditions. In general the critical volume of a nucleus is reduced by the heterogeneous site and thus facilitates nucleation. This depends on the catalytic activity, the wetting behavior of the melt on the heterogeneous site, and the size of the heterogeneous particles. This is reflected in a reduction of the average onset time for crystallization in an isothermal experiment compared to homogeneous

nucleation. The finding that at high temperatures the time to reach nucleation takes up to several thousand seconds showed that nucleation is still required. Therefore, the active size of the heterogeneities is smaller at high temperatures than the critical cluster radius. However, when the cross-over range is reached and the critical cluster radius is decreased the heterogeneous particles become overcritical. Therefore, spontaneously the samples are filled with nuclei at a density that corresponds to the density of the heterogeneous nucleation sites. These nuclei then simply grow with time. As soon as all nuclei start growing, the nucleation rate drops sharply since the remaining matrix is still very robust against homogeneous nucleation. This scenario is supported by microstructural investigations, where it was found that upon isothermal annealing at temperatures below 710 K the number of nuclei does not increase with time [19]. In order to fit the experimental results in the low temperature region, which has been performed for 703 and 628 K a much larger number of nuclei as given by the steady state rate is required that increases in this temperature range as opposed to the steady state rate. Following equation (4) for pre-existing nuclei the measured peaks can be best fitted with,  $N = 10^{20} \text{ m}^{-3}$  for 703 K and  $N = 10^{25} \text{ m}^{-3}$  for 628 K. Compare to the number of nuclei of  $N = 10^{16} \text{ m}^{-3}$  at 673 K derived from microstructural investigation of  $\text{Pd}_{40}\text{Ni}_{10}\text{Cu}_{30}\text{P}_{20}$  alloys [8] the fitted one is four orders of magnitude off. However, this agreement is satisfactory if we take into account that the number extracted from the fit depends sensitively on the parameters used for the calculations. If, for example, the diffusivity, which was obtained from the viscosity assuming the validity of the Einstein–Stokes equation, is one order of magnitude off, then the extracted  $N$  changes by three orders of magnitude. Considering the complexity of the crystallization mechanism the calculations represents a rough estimation which nevertheless accounts for the substantial part. In detail, there are still some discrepancies between the measured and calculated crystallization peak. For example, in a recently developed qualitative model by Bossuyt [24] it was claimed that for temperatures below the nose in the TTT diagram the heat release upon crystallization enhanced both, the nucleation and growth in the crystal neighborhood. This contribution would increase the crystallization rate and leads to a sharper increase of the crystallization event as observed in the experiment.

Preliminary experiments show that in higher purity  $\text{Pd}_{43}\text{Ni}_{10}\text{Cu}_{27}\text{P}_{20}$  a decrease of the temperature of the transition region to collective crystallization. This also supports the view, that spontaneous nucleation on catalysts initiates crystallization. Studies of other Pd-based alloys suggest as well that the crystallization

process is influenced by heterogeneities [15, 25].

Although the discussion of the experimental results favors that heterogeneous nucleation at impurities causes the spontaneous formation of the nuclei, a decomposition process or catastrophic nucleation cannot be excluded as an influencing factor to the observed transition. For Vit 1, where a decomposition process strongly influenced crystallization [22, 26, 27, 28] and impurities show only minor influence on the crystallization it has been found, that there is an undercooling level below which a history dependent crystallization takes place [29]. This transition temperature is closed to the “nose” temperature and for undercoolings above this temperature the results suggest the liquid remains unchanged whereas below an irreversible process takes place.

Even though the activation energy for nucleation is two orders of magnitude higher than the thermal energy in the transition temperature region, one has to keep in mind that the activation energy was calculated for a sharp interface. However, a diffuse interface [30] would result in a significantly lower activation energy. A study of the influence of the ingot purity and the fluxing with  $\text{B}_2\text{O}_3$  might enable to clarify the origin of the transition from nucleation to growth controlled crystallization.

## 5. CONCLUSIONS

In conclusion, the crystallization of  $\text{Pd}_{43}\text{Ni}_{10}\text{Cu}_{27}\text{P}_{20}$  was investigated under isothermal conditions in a DSC. These investigations allow us to determine the entire crystallization kinetics, i.e., the time to reach crystallization and the time for the actual crystallization process. This is represented in the crystallized volume fraction as a function of time and temperature and leads for the first time to the construction of a complete TTT-diagram for the transformation kinetic of an undercooled metallic melt into the crystalline state. This diagram reveals two different time scales. The peak width of the crystallization events increases over two orders of magnitude with decreasing temperatures. The time to reach crystallization shows a “nose” shape. Modeling the crystallization requires two different mechanisms. Describing the measured crystallization rate at low temperatures with a common isothermal model requires a large number of pre-existing nuclei. Crystallization at high temperatures can be best described by assuming a steady state nucleation process, which initiated crystallization and triggers further nucleation.

Statistical investigations were carried out by dividing the sample into up to 300 particles. The experimental results suggest a change in crystallization mechanism with a very sharp transition from high to low temperatures. At high temperatures an enormous scatter in the time to reach crystallization was observed. The time-scale to reach crystallization is up to three orders of magnitude larger than the time-scale

of the crystallization event. This suggests that the time to reach crystallization is nucleation controlled and the crystallization process itself causes further nucleation reflecting in the narrow crystallization peak. In the low temperature region very little scatter of  $t_{1\%}$  was observed in fluxed and unfluxed samples and is independent of the sample size. This suggests that the supercooled liquid becomes unstable with respect to the nucleation of crystals, which means that nuclei form spontaneously over the entire sample. This results in the fact that the growth of the crystals solely determines the time scale of the crystallization process. Describing the measured crystallization rate at low temperatures with a common isothermal model requires a large number of pre-existing nuclei.

*Acknowledgements*—This work was supported by the National Aeronautics and Space Administration (Grant No. NAG8-1744) and the Department of Energy (Grant No. DEFG-03086ER45242) (authors J.S and W.L.J). Y.W. thanks for support from Army Research Office (Grant No. DAAD19-99-1-0328). The authors express their gratitude to Michelle Giron and Masahiro Kuno for technical assistance.

#### REFERENCES

- Kui, H. W., Greer, A. L. and Turnbull, D., *Appl. Phys. Lett.*, 1984, **45**, 615.
- Inoue, A., Yamaguchi, H., Zhang, T. and Masumoto, T., *Mater. Trans. JIM*, 1990, **31**, 104.
- Inoue, A., Zhang, T. and Masumoto, T., *Mater. Trans. JIM*, 1990, **31**, 177.
- Peker, A. and Johnson, W. L., *Appl. Phys. Lett.*, 1993, **63**, 2342.
- Nishiyama, N. and Inoue, A., *Mater. Trans. JIM*, 1996, **37**, 1531.
- Lu, I. -R., Wilde, G., Görler, G. P. and Willnecker, R., *J. Non-Cryst. Solids*, 1999, **250–252**, 577.
- Kim, Y. J., Busch, R., Johnson, W. L., Rulison, A. J. and Rhim, W. K., *Appl. Phys. Lett.*, 1996, **68**, 1057.
- Loeffler, J., Schroers, J. and Johnson, W. L., *Appl. Phys. Lett.*, 2000, **77**, 681.
- Schroers, J., Busch, R. and Johnson, W. L., *Appl. Phys. Lett.*, 2000, **77**, 1158.
- Uhlmann, D. R., *J. Non-Cryst. Solids*, 1972, **7**, 337.
- Turnbull, D., *J. Chem. Phys.*, 1952, **20**, 411.
- Perepezko, J. H. and Paik, J. S., *J. Non-Cryst. Solids*, 1984, **61–62**, 113.
- Schroers, J., Busch, R. and Johnson, W. L., *Appl. Phys. Lett.*, 2000, **76**, 2343.
- Avrami, M., *J. Chem. Phys.*, 1939, **7**, 1103.
- Nishiyama, N. and Inoue, A., *Acta mater.*, 1999, **47**, 1487.
- Turnbull, D., *J. Appl. Phys.*, 1950, **21**, 1022.
- Holland-Moritz, D., Schroers, J., Herlach, D. M., Grushko, B. and Urban, K., *Acta mater.*, 1998, **5**, 1601.
- Jackson, K. A. and Hunt, J. D., *Trans. Metall. Soc. AIME*, 1966, **236**, 1129.
- Petarskaya, E., Schroers, J. and Johnson, W. L., *MRS 2000 proceedings*, in press.
- Schroers, J., Volkman, T., Herlach, D. M., Allen, D. R. and Perepezko, J. H., *Int. J. Rap. Sol.*, 1996, **9**, 267.
- Busch, R., Schneider, S., Peker, A. and Johnson, W. L., *Appl. Phys. Lett.*, 1995, **67**, 1544.
- Borchers, C., Busch, R., Schroers, J. and Johnson, W. L., 2000, *Acta mater.*, submitted for publication.
- Kuno, M., Busch, R. and Schroers, J., 2001, *Scripta mater.*, submitted for publication.
- Bossuyt, S., 2001, *Scripta mater.*, in press.
- Drehman, A. J. and Greer, A. L., *Acta metal.*, 1984, **32**, 323.
- Schneider, S., Thiyagarajan, P. and Johnson, W. L., *Appl. Phys. Lett.*, 1996, **68**, 493.
- Wang, W. -H., Wei, Q., Friedrich, S., Macht, M. P., Wand-erka, N. and Wollenberger, H., *Appl. Phys. Lett.*, 1997, **71**, 1053.
- Schroers, J., Busch, R., Masuhr, A. and Johnson, W. L., *Appl. Phys. Lett.*, 1999, **74**, 2806.
- Schroers, J. and Johnson, W. L., *J. Appl. Phys.*, 2000, **88**, 45.
- Granasy, L., *J. Non-Cryst. Solids*, 1993, **162**, 301.